Potential roughness near lithographically fabricated atom chips

P. Krüger,[1,2] L. M. Andersson,[1,3] S. Wildermuth,[1] S. Hofferberth,[1,4] E. Haller,[1] S. Aigner,[1] S. Groth,[1,5] I. Bar-Joseph,[5] and J. Schmiedmayer[1,4]

[1]*Physikalisches Institut, Universität Heidelberg, D-69120 Heidelberg, Germany*

[2]*Laboratoire Kastler Brossel, École Normale Supérieure, 24 Rue Lhomond, F-75005 Paris, France*

[3]*Department of Microelectronics and Information Technology, KTH, SE-164 40, Kista, Sweden*

[4]*Atominstitut der Österreichischen Universitäten, TU-Wien, A-1020 Vienna, Austria*

[5]*Department of Condensed Matter Physics, The Weizmann Institute of Science, Rehovot 76100, Israel*

(Received 30 December 2006; revised manuscript received 1 October 2007; published 28 December 2007)

Potential roughness has been reported to severely impair experiments in magnetic microtraps. We show that these obstacles can be overcome as we measure disorder potentials that are reduced by two orders of magnitude near lithographically patterned high-quality gold layers on semiconductor atom chip substrates. The spectrum of the remaining field variations exhibits a favorable scaling. A detailed analysis of the magnetic field roughness of a 100-μm-wide wire shows that these potentials stem from minute variations of the current flow caused by local properties of the wire rather than merely from rough edges. A technique for further reduction of potential roughness by several orders of magnitude based on time-orbiting magnetic fields is outlined.

DOI: 10.1103/PhysRevA.76.063621 PACS number(s): 03.75.Be, 39.90.+d

INTRODUCTION

Trapping and manipulating cold neutral atoms in microtraps near surfaces of atom chips is a promising approach toward a full quantum control of matter waves on small scales [1]. In a number of experiments, a large variety of potential configurations have been realized using combinations of current-carrying wires [2–8], electric [9], optical [10], and radio-frequency (rf) [11,12] fields. The tight confinement on atom chips allows for easy formation of Bose-Einstein condensates (BECs) [13–16]. Even coherent manipulation of matter waves in momentum [17,18] and position space [11,12,19] has been demonstrated.

To realize the full potential and versatility of microtraps, it is desirable to tailor potentials at a scale of 1 μm or below, for example to establish appreciable coupling between atoms located at neighboring sites of a trap array [20]. Since high spatial frequencies in electric and magnetic fields are exponentially damped ($\propto e^{-kd}$, where k is the spatial frequency and d the distance from the field source) when receding from the source of the fields, short distances to the surface of the chip are essential for achieving high-resolution complex potentials. While the fabrication of structure sizes below 1 μm is not problematic, unintended potential roughness has been reported to severely alter the trapping at surface distances $d < 100$ μm, resulting in a longitudinal fragmentation of (thermal) clouds, near both current-carrying [21–24] and permanent magnetic structures [25–28]. In the case of electromagnets, such large potential roughness has been observed in traps created by macroscopic wires and atom chips fabricated by electroplating techniques [29–31]. It has prevented the creation of tightly confined one dimensional (1D) quasi BECs on atom chips.

Here we show that, by employing an appropriate atom chip fabrication technique [32], experiments are no longer subject to such limitations [53]. The potential roughness near the chip surface is sufficiently small to allow for the preparation of continuous extremely elongated (aspect ratio >1000) 1D quasi-BECs (Fig. 1). These samples are in turn used to characterize the remaining disorder potentials with high sensitivity. In fact, this high field sensitivity of ultracold atoms has allowed initiation of the development of an atom-surface microscope [33,34].

I. EXPERIMENTAL SETUP

Our experimental apparatus is described in detail in [35,36]. The heart of our setup is a hybrid macroscopic-microscopic atom chip assembly [35]. It holds the macroscopic wire structures used to precool and capture the atoms in the primary phase of the experiment as well as the microstructures needed for cooling the sample to quantum degeneracy. A rich toolbox for the manipulation of cold atomic clouds and Bose-Einstein condensates is integrated onto the atom chip using appropriately designed wire structures [1].

The microstructures on the atom chip are fabricated on a 700 μm-thick silicon substrate using optical lithography and gold evaporation [32]. The process is optimized for tall wire structures (>1 μm) to increase the maximally sustainable

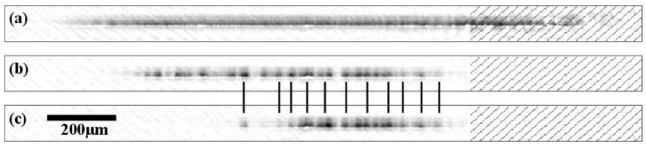

FIG. 1. *In situ* absorption images of atom clouds positioned at a chip-surface distance of ~ 5 μm above a current-carrying wire (cross section 3.1×10 μm^2). Parts of the images do not fully represent the atom density distribution since the imaging light beam was obstructed by bonding wires (hatched regions). (a) Thermal atoms show no fragmentation. (b) BECs display a much higher sensitivity and residual disorder potentials cause a fragmentation of the cloud. (c) A longitudinal displacement of the BEC by tuning the trapping potential shows that the disorder potential is stable in position.

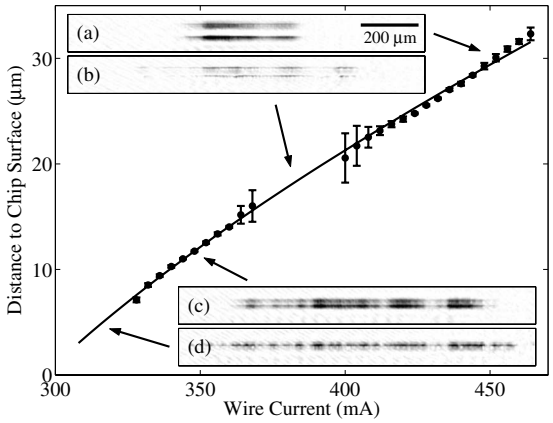

FIG. 2. Distance d of the BEC from the (mirror) chip surface as a function of wire current (3.1×100 μm^2 wire). Atoms near the surface produce a double image when illuminated by an inclined imaging beam as shown in the insets (a)–(c). The imaging beam together with the chip surface produces a fringe pattern that makes distance measurements less reliable for certain surface distances (b). For clouds closer than ~5 μm from the surface, the two images merge (d). To determine d also in these cases we use an extrapolation according to a best fit (solid line) with the exact bias field strength as the only fitting parameter. The fitting model takes the finite size of the wire into account.

current. The height of the wires used in the experiments described here was enhanced by repeating the lithographic process. The resulting total wire heights are 3.1 μm. Typical current densities in our experiments exceed 2×10^7 A/cm^2 without the risk of wire destruction.

The experimental procedure starts with typically 10^8 ^{87}Rb atoms accumulated in a mirror magneto-optical trap. The atoms are subsequently transferred to a purely magnetic trap and cooled to ~5 μK by radio-frequency (rf) evaporation. This sample of $\gtrsim10^6$ atoms is then loaded to the selected chip trap and location, where a second stage of rf evaporative cooling creates either a BEC or a thermal cloud just above the critical condensation temperature.

All information about the ultracold thermal or Bose-condensed atomic sample is extracted from resonant absorption imaging, performed on the $F=2\rightarrow F'=3$ transition. The atomic clouds are studied either *in situ* or after potential free time-of-flight expansion. They are imaged onto a charge-coupled device camera using standard precision acromats. The imaging has a diffraction-limited resolution of ~3 μm, and allows us to study quasi BECs with a linear density $n_{1D}>1$ atom/μm. For $n_{1D}>10$ atoms/μm the imaging is atom-shot-noise limited.

In order to determine the cloud's distance from the surface, d, we slightly incline the imaging beam with respect to the chip mirror surface by ~25 mrad. For sufficiently small d (<100 μm) this leads to a duplicated absorption image [16,37] (Fig. 2). *In situ* height measurements of trapped atomic clouds can be used to calibrate our magnetic fields. As our imaging resolution does not allow us to measure d for very close surface approaches ($d<5$ μm), we use the calibrated values of the bias fields together with the measured wire currents to infer d in these cases. At the tight confinement of our atom chip traps (from $\omega_\perp=2\pi\times3$ kHz up to $\omega_\perp>2\pi\times10$ kHz) the modification of the height due to atom-surface interactions can be neglected.

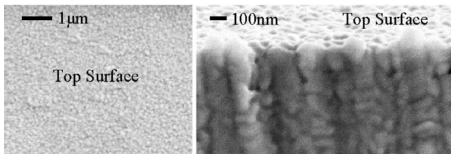

FIG. 3. Scanning electron microscope images of the chip wire surface (left) and edges (right). The grain sizes of less than 100 nm determine both the surface and edge roughness.

II. MEASUREMENT OF POTENTIAL ROUGHNESS

When we prepare an ultracold atomic ensemble very close to the current-carrying atom chip wires we observe the following: With thermal atoms we *always* (down to $d\sim2$ μm and cloud temperatures of less than 1 μK) measure a smooth longitudinal density profile, inside the trap [Fig. 1(a)] and in the time-of-flight images, independent of the wire used to form the trap and the position of the atomic cloud. This is in stark contrast to previous findings [21–24].

From averaging many pictures with ultracold thermal atoms [$T\sim1$ μK like the one shown in Fig. 1(a)] we can infer that the rms magnetic field roughness must be $\Delta B/B<10^{-4}$ for the 10-μm-wide wire. This limit applied to any wire studied on this chip.

When the atoms condense to a BEC, the measurement sensitivity is greatly enhanced [33,34]. Even at the level of this sensitivity, density variations of the elongated condensed cloud become discernable only for distances below $d<30$ μm [Figs. 2(a) and 2(c)]. The potentials are so smooth that we can create continuous 1D quasi-BECs ($\mu<0.5\hbar\omega_\perp$) of up to >1 mm length at down to $d\sim5$ μm surface distance and trapping frequencies of up to $\omega_\perp\sim2\pi\times10$ kHz.

We attribute the dramatic reduction of the disorder potentials to our atom chip fabrication method. We obtain chips with very smooth wire structures by adapting a standard microchip fabrication process to the production of our atom chips [32,38]. Masks written by electron beam lithography are used to structure a several micrometer thick, high-quality gold layer on a semiconductor wafer using a lift-off procedure. The result is a smooth gold mirror with precise gaps defining the current path in the wire (Fig. 3).

We have probed the residual potential roughness for various trapping geometries based on a 100-μm- and several 10-μm-wide wires at atom-surface distances down to 3 μm and transverse confinement of between $\omega_\perp=2\pi\times1$ kHz and $\omega_\perp>2\pi\times10$ kHz. For the quantitative analysis presented here, we take traps with a transverse confinement of $\omega_\perp\sim2\pi\times3$ kHz, extract longitudinal density profiles n_{1D} from the *in situ* absorption images, and calibrate them with the absolute atom number derived from time-of-flight images taken under equal experimental conditions. A comparison between the longitudinal density profiles of the trapped and the

released cloud after time-of-flight expansion shows that no detectable expansion occurs in the longitudinal direction.

The density profile $n_{1D}(z)$ can be converted into a map of the spatial profile of the longitudinal potential energy variations $V(z)$. For a pure 1D quasi-BEC the relevant energy scale is given by the chemical potential. The longitudinal potential can be calculated from the 1D density profile by

$$V_0 + V(z) = -\hbar\omega_{tr}\sqrt{1 + 4a_{scat}n_{1D}(z)}, \quad (1)$$

where a_{scat} is the s-wave scattering length (5.2 nm for ^{87}Rb) and V_0 is an arbitrary offset [34,39].

The above expression requires the 1D quasi-BEC to be in an equilibrium state. This may not be the case in our experiment over the entire length of the BEC ($\sim$1 mm). A variation of μ on large longitudinal length scales >200 μm can be maintained longer than the lifetime of the BEC if strong potential barriers separate the different fragments of the condensate (see also [40]). Therefore the longitudinal potential can only be accurately reconstructed if the condensate is continuous over the entire length of the trap. We ensure that this condition is satisfied by monitoring the $n_{1D}(z)$ profile and the reconstructed longitudinal potential variations throughout the lifetime of the condensate.

We have verified the size, the basic shape of our potentials, and their magnetic origin by radio-frequency spectroscopy of the trapped atoms. After production of the condensate, we apply a homogeneous rf field at a frequency ν close to that corresponding to the lowest energy in the trap ν_0. The frequency ν defines the maximum chemical potential μ of the entire condensate. As ν is lowered, the condensate starts to be depleted, the rf "cuts" into the BEC. Inhomogeneous μ of the cloud would then show as variations in the density profiles as a function of ν. This method of determining the potential curve suffers from the fact that it depends on the absolute value of the field. Consequently, it is very sensitive to the exact value of the trap bottom and cannot be used for full quantitative measurements. To achieve the same resolution for local small magnetic changes as in the BEC microscope [33,34], a stability of the trap bottom of better than 10 μG would be required.

From the images shown in Figs. 1(b) and 1(c) we find a rms magnetic field roughness of $\Delta B/B \sim 7\times10^{-5}$ for the 10-μm-wide wire at 5 μm height. This value is typical of the majority of the wires studied, even though in some rare cases we found large defects where the BEC preferentially accumulates.

The analysis in the following is exclusively based on absorption images of continuous 1D quasi BECs. Figure 4 shows a full map of disorder potentials as a function of distance from the surface of a 10 μm-wide wire.

III. ORIGIN OF POTENTIAL ROUGHNESS

The previously observed potential roughness [21–24] has been attributed to inhomogeneous magnetic field components ΔB in the direction *parallel* to the current-carrying wire creating the trapping field B_z. Such field components can be caused by variations in the current flow direction in the chip wires. Strongly confining trapping and guiding potentials on atom chips are formed by the subtraction of two magnetic fields, the field of a current-carrying wire and a (homogeneous) bias field (side guide configuration [41]). The remaining field at the potential minimum is determined by the angle between wire field and bias field. A small change of the current direction may thus result in a significant change in the trapping potential.

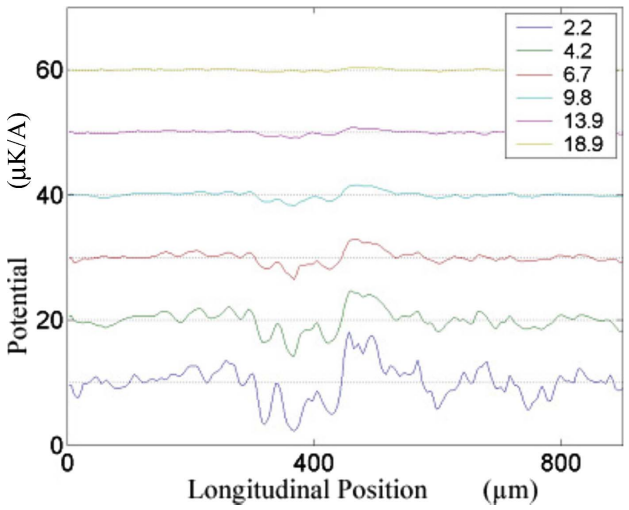

FIG. 4. (Color online) Disorder potential profiles for various heights over a 10-μm-wide wire surface. For comparison with previously published data, the units are given in μK/A and not in the universal $\Delta B/B$. Longitudinal profiles of the disorder potential for selected h (given in μm in the legend). Each curve has been shifted by 10 μK/A; the dotted lines represent the corresponding zero-potential level.

We have investigated the origin of the potential roughness by varying the cloud's global position along the longitudinal trapping axis (parallel to the trapping wire). We find that the local potential structure is very robust with respect to such a change [Figs. 1(b) and 1(c)]. This confirms that microscopic static properties of the trapping wire cause the condensate fragmentation.

To assess whether also this dramatically reduced potential roughness is magnetic in origin we have varied the wire current while adapting the bias field so that the BECs were trapped at fixed distances from the wire (Fig. 5). The reconstructed potential variations scale linearly with the current I in the wire down to the sensitivity limit of our measurements: $\Delta B/B \sim 3\times10^{-6}$. Consequently, we can exclude any current-independent sources of disorder potentials such as electrostatic patch effects [42] at the scale of $<10^{-13}$ eV for $d>5$ μm and conclude that the observed small potential variation stems from irregular current flow in the wire.

IV. EDGE ROUGHNESS VS LOCAL PROPERTIES OF THE WIRE

It has been suggested that current flow changes could be derived from fabrication inhomogeneities, surface roughness [43,44], and residual roughness of the wire borders [45]. The model of Wang *et al.* [45] provides a full quantitative expla-

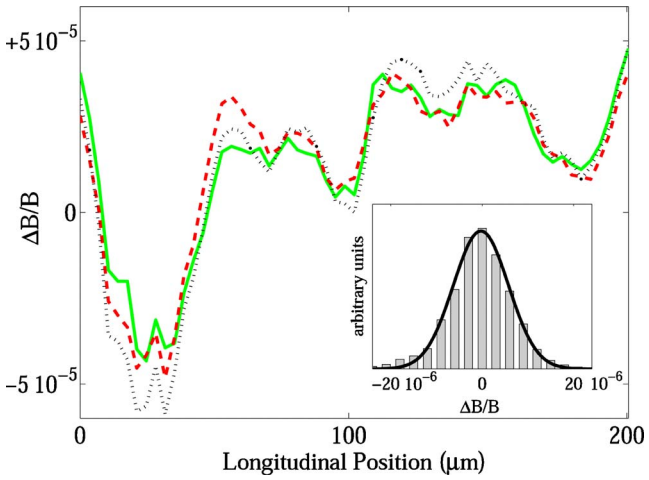

FIG. 5. (Color online) Longitudinal potential profiles measured with BECs at a constant distance of $d=10$ μm from the surface of the 100-μm-broad wire. The different traces were measured at different currents and are normalized to the corresponding trapping fields. The bias field (10, 20, and 30 G; black dotted, solid green, and dashed red lines, respectively) was adapted in order to keep d constant. The inset shows a histogram of the deviations of the curves. The width of the distribution ($\sigma \sim 8 \times 10^{-6}$) is similar to the shot-to-shot variations of different realizations of the same experiment with equal wire currents.

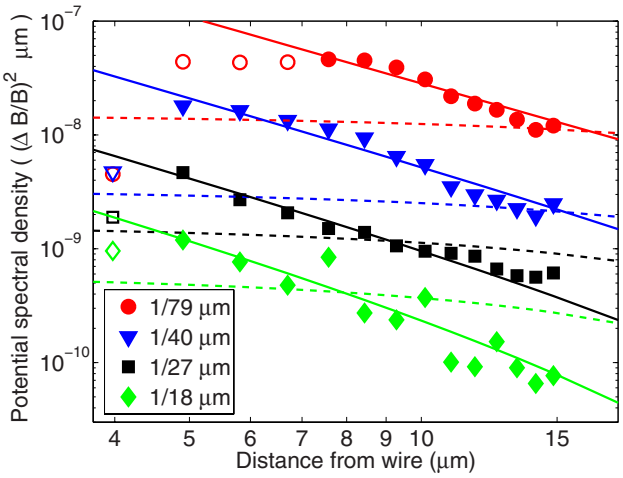

FIG. 6. (Color online) Spectral power density of the potential roughness near the 100-μm-wide gold wire for four spatial frequencies, measured at a transverse confinement of $\omega_\perp \sim 2\pi \times 3$ kHz. The open symbols correspond to data where the detected signal is limited by the chemical potential μ of the BEC. For these data points the complete depth of the potential cannot be measured, and they were omitted in the analysis. The solid lines are best fits according to a local fluctuating current path model; the dashed lines show best fits to the model outlined in [45]. For both models the only fitting parameter is the strength of the current path fluctuation at the corresponding spatial frequency k.

nation of the much larger potentials found near electroplated gold wires [24] based solely on wire edge roughness.

In order to study the source of the irregular current flow in our experiments we have performed two sets of measurements. First, we measure the variation of the potential roughness at the center of various wires with height. Here data from a 100-μm-wide wire are most relevant because a distinction between edge and local sources of irregular current flow is possible only for $d \lesssim w$. In a second experiment we measure the full potential landscape at 10 μm height above the same 100-μm-wide wire over its full width.

The main observation is that the scaling of the amplitude and the frequency spectrum of the disorder potentials with height d for wire widths between 10 and 100 μm are very similar. For $d < 50$ μm, this should not be the case if the roughness of the wire edge were the dominating cause as suggested in [45]. For the 100-μm-wide wire, Fig. 6 shows potential spectral densities (PSDs) of the disorder potential at four different spatial frequencies k. Over the whole range of heights d over which we observe potential roughness, the PSD scales for all frequency components more strongly with d than expected from the edge roughness model [45]. This rules out that the observed potential roughness is dominated by edge roughness.

Our observation is confirmed by measurements of the potential landscape over the whole width of the 100-μm-wide wire. We have performed these measurements by scanning the position of the condensate across the wire by appropriately adjusting the magnitude and direction of the external bias field. The reconstructed potential map contains information on possible additional effects caused by rough wire edges (Fig. 7). Even though the absolute value of the potential roughness PSD varies by many orders of magnitude as a function of spatial frequency, the roughness at each individual frequency is nearly constant over the whole wire width. With the exception of a single isolated spatial frequency, no significant increase near the wire edges is found.

Both observations clearly show that *local* current path deviations are dominant. These can be caused by inhomogeneous conductivity or top surface roughness [43,44]. A simple model taking local sources of current path deviations into account is a current flowing along a narrow irregular path below the atoms. We test this model by fitting the expected variation of the field roughness with d to the measured PSD. Here the spectrum of the current variation is left as a free fitting parameter. The model agrees reasonably with the data and reproduces the height dependence of the measured PSD over the entire investigated spectrum ($k > 1/200$ μm^{-1}). The local current flow fluctuation spectrum that results from the best fit scales as $\sim 1/k^2$.

In a more detailed model, the potential roughness is connected to the the 2D current flow in the wire. The complete measurement of the z component of the magnetic field over the whole wire allows us to reconstruct the y component of the 2D current density [33,34]. Figure 8 shows a comparison of the height dependence of the measured power spectral density of the relative magnetic field fluctuations in the center of the 100 μm wire, with the PSD calculated from the current density reconstructed from the measurements at 10 μm height. For the comparison between calculation and experiment we added a 3 nT white noise to the reconstructed magnetic field to account for the actual magnetic field measurement noise as determined experimentally (Fig. 5). The

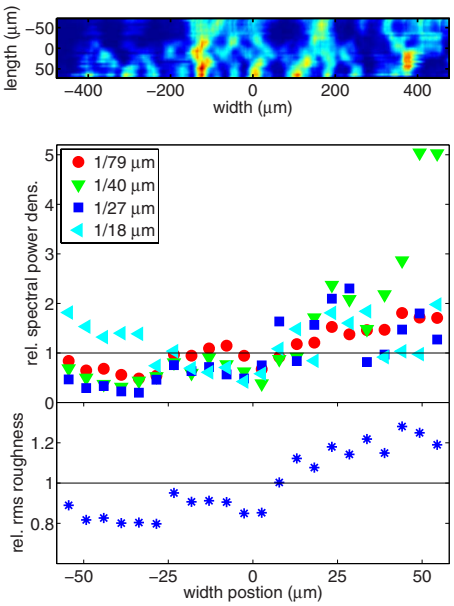

FIG. 7. (Color online) Potential roughness measurements 10 μm above the the 100-μm-wide gold wire. Top: False color potential map recontructed from many 1D quasi-BEC images. Bottom: Change of the spectral power density of the potential roughness over the width of the 100-μm-wide wire for four spatial frequencies. For most of the frequencies the distribution is flat, except for $k=1/40$ μm, where an increase is apparent when the wire edge is approached. We interpret this as caused by specific local defects in the edge.

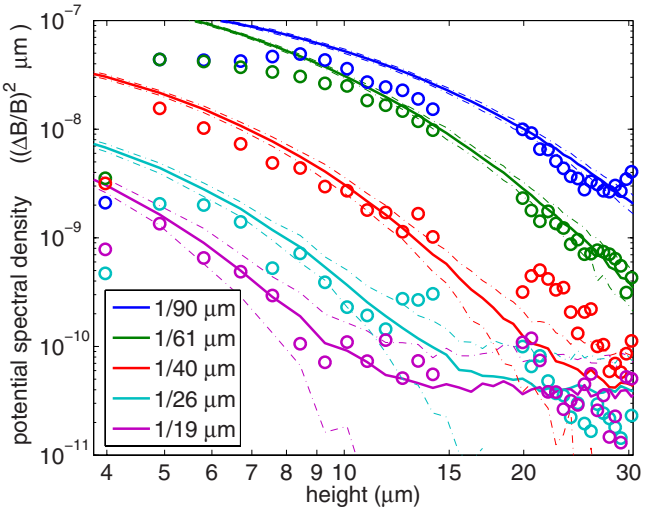

FIG. 8. (Color online) Height dependence of the potential roughness in the center of the 100-μm-wide gold wire are compared to the potential roughness calculated from the current reconstructed from the measurement of the magnetic field at 10 μm above the the 100 μm wire. The potential power spectral density calculated from the reconstructed current and a 2σ band is compared to the measured data. The 2σ band is estimated from the 3 nT magnetic field resolution for a single-shot single-point measurement with 3.5 μm spatial resolution.

calculated noise floor of the measurement is then also consistent with the measured noise floor in the evaluated PSD. To illustrate the statistical uncertainty in the measured PSD we calculated 2σ bands, which are indicated by the dash-dotted lines.

We find remarkably good agreement over the whole height range, even at heights below 10 μm. This good agreement below 10 μm can be attributed to the particularly smooth potential at small length scale, as already indicated by the simple local current flow model, which is consistent with $a \sim 1/k^2$ scaling of the irregular current flow. Such scaling favors small length scales where the magnetic field roughness is smaller than our highly sensitive detection threshold.

To reach a more detailed understanding of the local current flow deviations we have found, microscopically well-characterized wires will have to be fabricated and tested. A distinction between surface roughness and bulk effects requires measurements in a regime where the distance between atoms and wire surface is comparable to or smaller than the wire height. To study effects of surface roughness one would need to measure the top and bottom surfaces of the wire with better than 1 nm precision over the whole measurement range of 100×1000 μm^2.

V. COMPARISON TO OTHER ATOM CHIPS

We now compare our results to the potential roughness measured for other chips in different experiments. The most direct comparison can be done with the Orsay experiment [24,44] where detailed measurements are available for $d > 35$ μm. Our data set extends to a surface distance of $d \sim 35$ μm; at higher distances the roughness becomes smaller than our detection threshold, even in the case of highly sensitive 1D quasi-BEC probes. At a surface distance of $d = 10$ μm, we find the rms $\Delta B/B = 3 \times 10^{-5}$ ($< 10^{-5}$) for spatial frequencies $k > 1/200$ μm^{-1} ($k > 1/50$ μm^{-1}). At $d > 35$ μm, where disorder potentials near electroplated wires have been measured, we find $\Delta B/B < 3 \times 10^{-6}$. This corresponds to a reduction by at least two orders of magnitude compared to [24,44].

The most detailed analysis of the Orsay data is given by the evaluation of the power spectral density of the $\Delta B/B$ roughness in [44]. Figure 9 shows a direct comparison between a similar analysis of our data and [44]. The measurements on our chip at 25 μm show a 3–4 orders of magnitude smaller power in the roughness fluctuation spectrum, in good agreement with the above observation.

In Fig. 10 we show a quantitative comparison between measurements we have made for various wires and data taken from the Orsay group and from other published experiments. In some cases, only potential profiles of the rms roughness of the potential are given and we had to infer the relevant quantity $\Delta B/B$ from these data in order to make the comparison meaningful.

VI. FURTHER REDUCTION OF POTENTIAL ROUGHNESS

The remaining potential roughness can be further reduced by a time-averaging method. Kraft *et al.* [46] proposed to

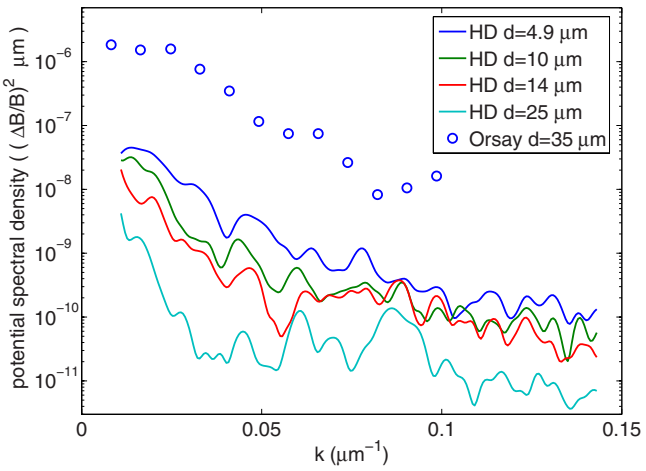

FIG. 9. (Color online) Comparison of the analysis of our 2003/04 data [53] presented in this work with the most detailed analysis of a different atom chip: the experiments at Orsay [44].

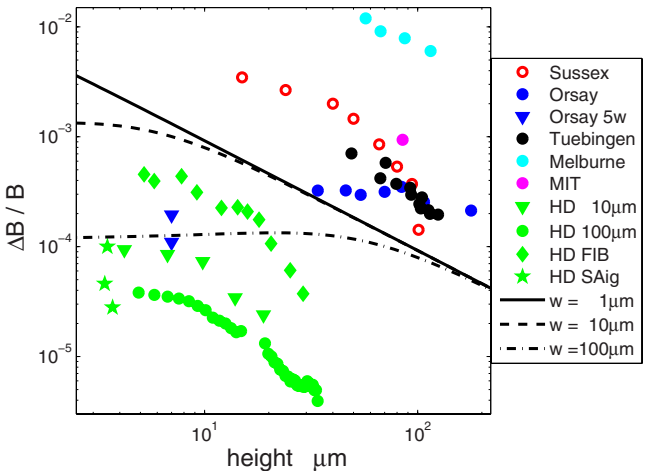

FIG. 10. (Color online) Comparison of all atom chip potential roughness measurements available to us. Most of the data are taken from the figures in the published literature and available Ph.D. theses. The color codes correspond different experimental groups, as indicated in the legend. Filled symbols denote rms values, data displayed as open symbols correspond to the peak-to-valley maximum height of the roughness. Sussex: data from a gold-coated wire [23]. Orsay: ○, show the data from an electroplated wire [24,44], more recent data from an evaporated gold chip shown as ▽ (peak to valley). Tübingen: data from electroplated wires [50]. Melbourne: data from a permanent magnet atom chip [28]. MIT: data from electroplated wires [15]. Heidelberg (2003/04 data [53]): data from the 100 μm wire shown as ○; data from the 10 μm wire shown as ◇ [36]. Later data from different other evaporated gold chip wires are shown as follows: The highest ever observed roughness in our atom chips: a 10 μm wire from ◇ [51]: Recent data from three different wires used in [52] *. The lines show the limits of maximal roughness allowed to be able to reach the one-dimensional regime of $\mu < \hbar\omega_\perp$ for different wire widths.

reduce the potential roughness by oscillating the wire current, and thereby averaging the unwanted longitudinal field components. This requires a special chip design since the bias field forming the trap also has to oscillate exactly in phase to maintain the transverse confinement. This idea was recently successfully implemented by Trebbia *et al.* [47].

Here we propose a different method to reduce the potential roughness by applying a technique based on time-orbiting potentials (TOPs) [48], and an orthogonal rotating rf field.

Without loss of generality we align the long axis of the trap (guide), and with it the current in the chip wire and the Ioffe field B_I, along the z direction. The potential roughness then stems from small magnetic field variations ΔB_z which result in a change of the potential $V=\mu(B_I+\Delta B_z)$ at the trap center.

To this trapping field we add an orthogonal TOP field rotating in the x-y plane,

$$\mathbf{B}_{\mathrm{TOP}}(t) = b_{\mathrm{rf}}(\hat{e}_x \cos \omega t + \hat{e}_y \sin \omega t), \tag{2}$$

where ω is chosen so small that the adiabatic approximation is still valid for the spin but where it is large compared to the trap frequency $\omega_\perp$. Under these conditions the effective potential is given by the time average of the instantaneous magnetic potential $V=\langle \boldsymbol{\mu}\cdot\mathbf{B}(t)\rangle_t$, where $\langle\ \rangle_t$ denotes the time average over a period of the trapping frequency [48].

Adding a small static perturbation $\delta\mathbf{B}=(\delta b_x, \delta b_y, \delta b_z)$ to the TOP field leads to an effective potential

$$\begin{aligned} V &= \langle \boldsymbol{\mu}\cdot(\mathbf{B}_{\mathrm{TOP}}(t)+\delta\mathbf{B})\rangle_t \\ &= \langle \mu\sqrt{(\delta b_x + b_{\mathrm{rf}}\cos\omega t)^2 + (\delta b_y + b_{\mathrm{rf}}\sin\omega t)^2 + \delta b_z^2}\rangle_t \\ &= \mu\left[b_{\mathrm{rf}} + O\left(\frac{|\delta\mathbf{B}|^2}{b_{\mathrm{rf}}}\right)\right]. \end{aligned}$$

In a side guide configuration, the standard building block of atom chip traps, the two in-plane components δb_x and δb_y are always zero at the minimum of the guide, and only the longitudinal field δb_z has to be considered. In our case $\delta b_z = B_I + \Delta B_z$. The effect of the potential roughness ΔB_z can now be minimized by reducing the Ioffe field B_I to zero (possible as a TOP trap can operate without a constant offset field), leaving only ΔB_z as the perturbation. In this case ($B_I=0$) the potential roughness is reduced by a factor $\Delta B_z/b_{\mathrm{rf}}$.

For typical parameters achievable on our atom chips ($b_{\mathrm{rf}} \sim 1$ G and $\Delta B_z \sim 1$ mG) the corrugations in a TOP trap are reduced by a factor of 1000 as compared to a Ioffe-Pritchard trap. The resulting potential roughness would correspond to $\sim$1 Hz. In addition, the longitudinal confinement of the trap will be reduced. This situation is ideally suited for studies of strongly correlated 1D systems approaching the Tonks-Girardeau limit [49].

As an example, we compare a typical potential with residual roughness taken from our experiments with the smoothed potential that would be achieved by subtracting the static Ioffe field and replacing it by an oscillating TOP field (Fig. 11).

CONCLUSION

To conclude, we have created single continuous 1D quasi-BECs on atom chips. We have used these 1D quasi-BECs to

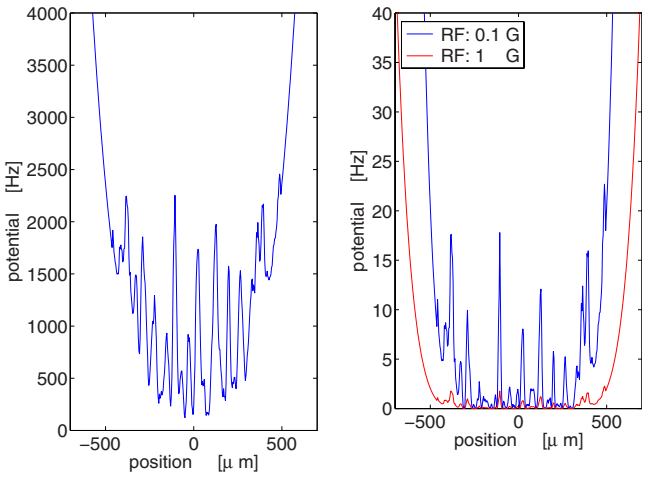

FIG. 11. (Color online) Reduction of the potential roughness on applying an oscillating rf near field. Left: Trap potential with original roughness. Right: Effective potential created by subtracting the Ioffe offset field and adding a rf field with 0.1 (1) G amplitude.

investigate the potential roughness near our lithographically fabricated current-carrying wires. The residual roughness has to be attributed to local properties of the wires resulting in irregular current flow at the scale of angular deviations from the nominal path of less than 10^{-4} rad. The measured potential roughness is two orders of magnitude smaller than previously observed in other atom chip experiments. The strong scaling of the magnetic field fluctuations with spatial frequency ($\sim 1/k^2$) indicates a dominance of large-scale inhomogeneities. The smallness of the high-frequency fluctuations opens up the way to micrometer-scale quantum manipulation on atom chips. Utilizing time-orbiting potentials promises to reduce the potential roughness by yet another three orders of magnitude.

ACKNOWLEDGMENTS

We thank M. Brajdic and L. Della Pietra for help in the experiments. This work was supported by the European Union, Contract No. IST-2001-38863 (ACQP), No. HPMF-CT-2002-02022, and No. HPRI-CT-1999-00114 (LSF) EU Transnational Access program, EU Project No. RITA-CT-2003-506095, and Integrated Project SCALA and the Deutsche Forschungsgemeinschaft, Contract No. SCHM 1599/1-1. P.K. acknowledges support by the Alexander von Humboldt Foundation and the EU, Contract No. MEIF-CT-2006-025047.

[1] R. Folman, P. Krüger, J. Schmiedmayer, J. Denschlag, and C. Henkel, Adv. At., Mol., Opt. Phys. **48**, 263 (2002).
[2] J. Reichel, W. Hänsel, and T. W. Hänsch, Phys. Rev. Lett. **83**, 3398 (1999).
[3] W. Hänsel, J. Reichel, P. Hommelhoff, and T. W. Hänsch, Phys. Rev. A **64**, 063607 (2001).
[4] J. Reichel, Appl. Phys. B: Lasers Opt. **74**, 469 (2002).
[5] D. Müller, D. Z. Anderson, R. J. Grow, P. D. D. Schwindt, and E. A. Cornell, Phys. Rev. Lett. **83**, 5194 (1999).
[6] N. H. Dekker, C. S. Lee, V. Lorent, J. H. Thywissen, S. P. Smith, M. Drndic, R. M. Westervelt, and M. Prentiss, Phys. Rev. Lett. **84**, 1124 (2000).
[7] R. Folman, P. Krüger, D. Cassettari, B. Hessmo, T. Maier, and J. Schmiedmayer, Phys. Rev. Lett. **84**, 4749 (2000).
[8] D. Cassettari, B. Hessmo, R. Folman, T. Maier, and J. Schmiedmayer, Phys. Rev. Lett. **85**, 5483 (2000).
[9] P. Krüger, X. Luo, M. W. Klein, K. Brugger, A. Haase, S. Wildermuth, S. Groth, I. Bar-Joseph, R. Folman, and J. Schmiedmayer, Phys. Rev. Lett. **91**, 233201 (2003).
[10] D. Gallego, Diplomarbeit, University of Heidelberg, 2005.
[11] T. Schumm, S. Hofferberth, L. M. Andersson, S. Wildermuth, S. Groth, I. Bar-Joseph, J. Schmiedmayer, and P. Krüger, Nat. Phys. **1**, 57 (2005).
[12] S. Hofferberth, I. Lesanovsky, B. Fischer, J. Verdu, and J. Schmiedmayer, Nat. Phys. **2**, 710 (2006).
[13] H. Ott, J. Fortagh, G. Schlotterbeck, A. Grossmann, and C. Zimmermann, Phys. Rev. Lett. **87**, 230401 (2001).
[14] W. Hänsel, P. Hommelhoff, T. W. Hänsch, and J. Reichel, Nature (London) **413**, 498 (2001).
[15] A. E. Leanhardt, A. P. Chikkatur, D. Kielpinski, Y. Shin, T. L. Gustavson, W. Ketterle, and D. E. Pritchard, Phys. Rev. Lett. **89**, 040401 (2002).
[16] S. Schneider, A. Kasper, C. vom Hagen, M. Bartenstein, B. Engeser, T. Schumm, I. Bar-Joseph, R. Folman, L. Feenstra, and J. Schmiedmayer, Phys. Rev. A **67**, 023612 (2003).
[17] A. Günther, S. Kraft, M. Kemmler, D. Koelle, R. Kleiner, C. Zimmermann, and J. Fortagh, Phys. Rev. Lett. **95**, 170405 (2005).
[18] Y. Wang, D. Anderson, V. Bright, E. Cornell, Q. Diot, T. Kishimoto, M. Prentiss, R. Saravanan, S. Segal, and S. Wu, Phys. Rev. Lett. **94**, 090405 (2005).
[19] S. Hofferberth, I. Lesanovsky, B. Fischer, T. Schumm, and J. Schmiedmayer, Nature (London) **449**, 324 (2007).
[20] T. Calarco, E. A. Hinds, D. Jaksch, J. Schmiedmayer, J. I. Cirac, and P. Zoller, Phys. Rev. A **61**, 022304 (2000).
[21] J. Fortagh, H. Ott, S. Kraft, A. Günther, and C. Zimmermann, Phys. Rev. A **66**, 041604(R) (2002).
[22] A. E. Leanhardt, Y. Shin, A. P. Chikkatur, D. Kielpinski, W. Ketterle, and D. E. Pritchard, Phys. Rev. Lett. **90**, 100404 (2003).
[23] M. P. A. Jones, C. J. Vale, D. Sahagun, B. V. Hall, and E. A. Hinds, Phys. Rev. Lett. **91**, 080401 (2003).
[24] J. Estève, C. Aussibal, T. Schumm, C. Figl, D. Mailly, I. Bouchoule, C. I. Westbrook, and A. Aspect, Phys. Rev. A **70**, 043629 (2004).
[25] M. Boyd, E. W. Streed, P. Medley, G. K. Campbell, J. Mun, W. Ketterle, and D. E. Pritchard, Phys. Rev. A **76**, 043624 (2007).
[26] C. D. J. Sinclair, J. A. Retter, E. A. Curtis, B. V. Hall, I. Llorente-Garcia, S. Eriksson, B. E. Sauer, and E. A. Hinds, Eur. Phys. J. D **35**, 105 (2005).
[27] B. V. Hall, S. Whitlock, F. Scharnberg, P. Hannaford, and A. Sidorov, in *Laser Spectroscopy XVII*, edited by E. A. Hinds, A.

Ferguson, and E. Riis (World Scientific, Singapore, 2005).
[28] S. Whitlock, B. V. Hall, T. Roach, R. Anderson, M. Volk, P. Hannaford, and A. I. Sidorov, Phys. Rev. A **75**, 043602 (2007).
[29] M. Drndić, K. S. Johnson, J. H. Thywissen, M. Prentiss, and R. M. Westervelt, Appl. Phys. Lett. **72**, 2906 (1998).
[30] J. Fortagh *et al.*, Appl. Phys. Lett. **81**, 1146 (2002).
[31] B. Lev, Quantum Inf. Comput. **3**, 450 (2003).
[32] S. Groth *et al.*, Appl. Phys. Lett. **85**, 2980 (2004).
[33] S. Wildermuth, S. Hofferberth, I. Lesanovsky, E. Haller, L. M. Andersson, S. Groth, I. Bar-Joseph, P. Krüger, and J. Schmiedmayer, Nature (London) **435**, 440 (2005).
[34] S. Wildermuth, S. Hofferberth, I. Lesanovsky, S. Groth, P. Krüger, J. Schmiedmayer, and I. Bar-Joseph, Appl. Phys. Lett. **88**, 264103 (2006).
[35] S. Wildermuth, P. Krüger, C. Becker, M. Brajdic, S. Haupt, A. Kasper, R. Folman, and J. Schmiedmayer, Phys. Rev. A **69**, 030901(R) (2004).
[36] P. Krüger, Ph.D. thesis, University of Heidelberg, 2004.
[37] S. Hofferberth *et al.* (unpublished).
[38] This fabrication method [32] was used for the chips in all our previous experiments [7–9].
[39] F. Gerbier, Europhys. Lett. **66**, 771 (2004).
[40] Y. Shin, M. Saba, A. Schirotzek, T. A. Pasquini, A. E. Leanhardt, D. E. Pritchard, and W. Ketterle, Phys. Rev. Lett. **92**, 150401 (2004).
[41] J. Denschlag, D. Cassettari, and J. Schmiedmayer, Phys. Rev. Lett. **82**, 2014 (1999).
[42] J. M. McGuirk, D. M. Harber, J. M. Obrecht, and E. A. Cornell, Phys. Rev. A **69**, 062905 (2004).
[43] A. Kasper *et al.*, J. Opt. B: Quantum Semiclassical Opt. **5**, S143 (2003).
[44] T. Schumm *et al.*, Eur. Phys. J. D **32**, 171–180 (2005).
[45] D.-W. Wang, M. D. Lukin, and E. Demler, Phys. Rev. Lett. **92**, 076802 (2004).
[46] S. Kraft *et al.*, J. Phys. B **35**, L469 (2002).
[47] J.-B. Trebbia, C. L. Garrido-Alzar, R. Cornelussen, C. I. Westbrook, and I. Bouchoule, Phys. Rev. Lett. **98**, 263201 (2007).
[48] W. Petrich, M. H. Anderson, J. R. Ensher, and E. A. Cornell, Phys. Rev. Lett. **74**, 3352 (1995).
[49] T. Kinoshita, T. Wenger, and D. S. Weiss, Science **305**, 1125 (2004).
[50] J. Forthagh, Ph.D. thesis, Universität Tübingen, 2003.
[51] L. Della Pietra, Ph.D. thesis, Universität Heidelberg, 2007.
[52] S. Aigner, Ph.D. thesis, Universität Heidelberg, 2007.
[53] P. Krüger, e-print arXiv:cond-mat/0504686.